BEHAVIORAL NEUROSCIENCE

Unitized representation of paired objects in area 35 of the macaque perirhinal cortex

Ryoko Fujimichi, Yuji Naya,* Kenji W. Koyano, Masaki Takeda, Daigo Takeuchi and Yasushi Miyashita
Department of Physiology, The University of Tokyo School of Medicine, 7-3-1 Hongo, Bunkyo-ku, Tokyo 113-0033, Japan

Abstract

The perirhinal cortex, which is critical for long-term stimulus–stimulus associative memory, consists of two cytoarchitectonically distinct subdivisions: area 35 (A35) and area 36 (A36). Previous electrophysiological studies suggested that macaque A36 is involved in both association and retrieval processes during a visual pair-association task. However, the neuronal properties of macaque A35 have never been examined because A35 is located in a very narrow region, which makes it difficult to systematically record single-unit activity from there. In the present study, we overcame this technical difficulty for targeting A35 by combining magnetic resonance imaging-guided *in-vivo* localization with postmortem histological localization. This two-track approach enabled us to record from 181 A35 neurons in two macaque monkeys while they performed a pair-association task. Among these neurons, 64 showed stimulus-selective responses during the cue period (cue-selective neurons), whereas 18 did during the delay period (delay-selective neurons). As in A36, the responses of cue-selective neurons in A35 to paired associates were correlated. In both areas, these correlations were stronger in neurons showing delay selectivity than in those without delay selectivity. Notably, delay-selective neurons in A35 responded similarly to the optimal stimulus and its paired associate, whereas delay-selective neurons in A36 discriminated between them. However, these neurons in both areas discriminated the primary pair, consisting of the optimal stimulus and its paired associate, from other pairs, indicating that selectivity across pairs was maintained between the two areas. These results suggest that delay-selective neurons in A35 represent these paired stimuli as a single unitized item rather than two associated items.

Introduction

The perirhinal (PRh) cortex is located at a pivotal point where the ventral visual stream meets the medial temporal lobe memory system, and is critical for various cognitive functions with its high-level object representations, particularly with the long-term representations of stimulus–stimulus associative memories (Miyashita, 1993, 2004; Murray *et al.*, 1993; Buckley & Gaffan, 1998; Buffalo *et al.*, 1999; Bussey & Saksida, 2005). It has been suggested that the relationships between associated items are represented by the responses of individual PRh cortex neurons (Miyashita, 1988; Sakai & Miyashita, 1991; Messinger *et al.*, 2001). A further study recorded neuronal activity from one of the two subdivisions in the PRh cortex, area 36 (A36), and its lateral adjacent region, area TE, to compare their relative contributions in pair-association (PA) memory (Naya *et al.*, 2003a). The results revealed that association between representations of the paired associates proceeds forward from area TE to A36. The other subdivision of the PRh cortex, area 35 (A35), is located medial to A36 (Fig. 1a). Structurally, A35 differs from A36 in that it lacks

layer IV and contains large darkly stained cells in layer V (Suzuki & Amaral, 2003a). These structural discontinuities provide a possibility that these two subdivisions make functionally different contributions to PA memory. However, the functional properties of A35 neurons have never been systematically examined in behaving animals. To date, examination of A35 neuronal activity has been largely limited to *in-vitro* studies (Cho *et al.*, 2000; de Curtis & Paré, 2004).

One plausible reason for the paucity of studies on A35 neurons is that A35 is located within the deep brain structure (Fig. 1a), which makes it difficult to systematically record single-unit activities there in behaving animals. We used a two-track approach to overcome this technical difficulty. (i) Before recording experiments, magnetic resonance (MR)-detectable metal deposits were made using an elgiloy microelectrode (Fig. 1b, left). The position of the elgiloy microelectrode was also visualized on X-rays, so that the metal deposits provided common references between the X-rays and MR images. During daily recording sessions, we visualized every tungsten microelectrode on X-rays, and thereby overlaid the electrode position on the MR image. (ii) At the end of the recording experiments, several electrolytic microlesions were made for reconstruction of the recorded sites and postmortem verification (Fig. 1c–h).

To investigate the mnemonic properties of A35 neurons, we trained two monkeys in a PA task, which required formation of an associative memory between two items. We found that visual responses to the

Correspondence: Yasushi Miyashita, as above.
E-mail: yasushi_miyashita@m.u-tokyo.ac.jp

Present address: Center for Neural Science, New York University, Washington Place, Room 809, New York, NY 10003, USA.

paired associates were strongly correlated in A35, as in A36, and this correlation was much stronger if the neurons showed stimulus selectivity during delay period. However, unlike delay-selective neurons in A36, those in A35 did not differentiate between the optimal stimulus and its paired associate, suggesting that delay-selective A35 neurons treat these paired stimuli as a single unitized item. The result implies that, considering its anatomical location at the crossing between visual and mnemonic processing, A35 neurons could play a role in abstracting a unitized representation from multiple behaviorally-related visual objects through long-term memory.

Materials and methods

Subjects and surgery

All animal procedures complied with the National Institutes of Health Guide for the Care and Use of Laboratory Animals and were approved by the Institutional Review Committee of the University of Tokyo School of Medicine. The subjects were two adult monkeys (*Macaca fuscata*, weighing 9.5–11 kg). The implantation of an MR-compatible head holder and chamber (Toei Plastic, Inc., Tokyo, Japan) for microelectrode recording to the skull followed standard aseptic, anesthetic and postoperative treatment protocols (anesthetic: sodium pentobarbital 2.5 mg/kg/h, i.v. and xylazine 2 mg/kg, i.m. supplemented as needed; analgesic: acetaminophen 20 mg/kg/day, p.o.; prophylactic antibiotic: ampicillin 100 mg/kg/day, i.m. or enrofloxacin 5 mg/kg/day, s.c.). Blood pressure, heart rate and oxygen saturation were all monitored continuously during the surgery. MR-compatible plastic screws (KYOCERA Corporation, Kyoto, Japan) were used to secure the head holder to the skull (Koyama *et al.*, 2004).

Behavioral task, electrophysiology and magnetic resonance imaging

To access neuronal responses in A35, we used a PA task that required formation of an associative memory between two items. The procedure for the PA task was described in detail previously (Sakai & Miyashita, 1991; Naya *et al.*, 2003a). The visual stimuli were 16 monochrome Fourier descriptors and geometrically distinct patterns were sorted into eight pairs. The combination of the paired associates was not predictable without memorizing them beforehand. Two monkeys were trained to memorize a set of eight pairs through repeated trials in the PA task. In each trial, one cue stimulus was presented on a PC monitor for 300 ms. After a 2-s delay interval, two choice stimuli, i.e. the paired associate of the cue stimulus (target) and one from a different pair (distractor), were presented (Fig. 2). The monkey obtained fruit juice as a reward for correctly touching the paired associate within 1.2 s. In the recording sessions after training, each monkey performed the PA task with more than 95% correct responses.

The procedure for single-unit recording was also described in detail previously (Sakai & Miyashita, 1991; Naya *et al.*, 2003a). The activity of single neurons was recorded extracellularly from one hemisphere in each monkey using a glass-insulated tungsten microelectrode. The microelectrode was inserted vertically into the target region through the intact dura mater along a stainless steel guide tube using a hydraulic microdrive manipulator (Narishige, Tokyo, Japan). We recorded from the first well-isolated neuron encountered while searching for the next neuron along each penetration of the microelectrode. The location of each electrode track was determined using X-ray images (Higuchi & Miyashita, 1996; Naya *et al.*, 2003a).

To obtain high-resolution structural images of each monkey's brain, a 4.7-T magnetic resonance imaging (MRI) scanner (Biospec 47/40; Bruker, Ettlingen, Germany) and 100 mT/m actively shielded gradient coils were used (Matsui *et al.*, 2007). The images were acquired under anesthesia using both the three-dimensional-modified driven equilibrium Fourier transform sequence and the inversion-recovery fast spin-echo sequence (echo time, 11.2 ms; repetition time, 4 s; inversion time, 300 ms; in-plane resolution, $375 \times 375 \ \mu m^2$; slice thickness, 1500 μm). Three-dimensional brain atlases were then constructed using MRIcro software (http://www.cabiatl.com/mricro/mricro/index.html).

Strategy for targeting area 35

Because A35 is a narrow strip of the cortex located within the fundus of the rhinal sulcus, it was a challenge to record single-unit activities from A35. We therefore used two approaches to accurately localize the recording sites.

Approach 1: in-vivo *localization of recording sites using magnetic resonance imaging-detectable metal deposit markers*

To increase the accuracy of our estimations of the microelectrode position *in vivo*, we aligned the physiological recording profiles with high-resolution MR images using MRI-detectable markers (Fung *et al.*, 1998; Koyano *et al.*, 2008; see other approaches in Matsui *et al.*, 2007; Cox *et al.*, 2008). To place these MRI-detectable markers, before starting a series of daily single-unit recording experiments, a glass-coated elgiloy microelectrode was inserted into the recording region in the direction parallel to the dorsoventral axis. The anteroposterior/lateromedial coordinates of the microelectrode were obtained from X-ray images, and the dorsoventral coordinate of the microelectrode tip was obtained from manipulator measurements (Naya *et al.*, 2003a). Small metal deposits were then made just above the fundus of the rhinal sulcus (part of the amygdaloid complex) by passing a direct anodic 4-μA current for 5 min. High-resolution structural MR images of the monkey brain were then obtained using a 4.7-T MRI scanner to detect the metal deposits. During daily recording sessions, the coordinates of the tungsten microelectrodes in the physiological recording profiles were determined from X-ray and manipulator measurements using the same procedure as used for the elgiloy microelectrode. Because the metal deposits had the three-dimensional coordinates on the MRI in addition to the three-dimensional coordinates on the X-ray images, these MRI-detectable deposits then served as common references that enabled us to establish a direct correspondence between these three-dimensional coordinates of the daily-recording sites and the brain structures on the MR images.

Approach 2: postmortem localization of recording sites using electrolytic lesion markers

At the end of the recording experiments, at least four small electrolytic lesions were created for postmortem verification of the microelectrode tip position in each monkey by passing a direct current (10 μA for 30 s) through the microelectrode (for the visualization of the microlesions, see Histology section below). These microlesions were employed to reconstruct the locations of the other recording sites using a linear interpolation method (Naya *et al.*, 2003a; Yoshida *et al.*, 2003). In one monkey, one of the microlesions was made at the point where the microelectrode track crossed the border between the white matter and gray matter (Fig. 1e, upper star). Another microlesion was placed within A35 (Fig. 1e, lower star). In another monkey, two of the
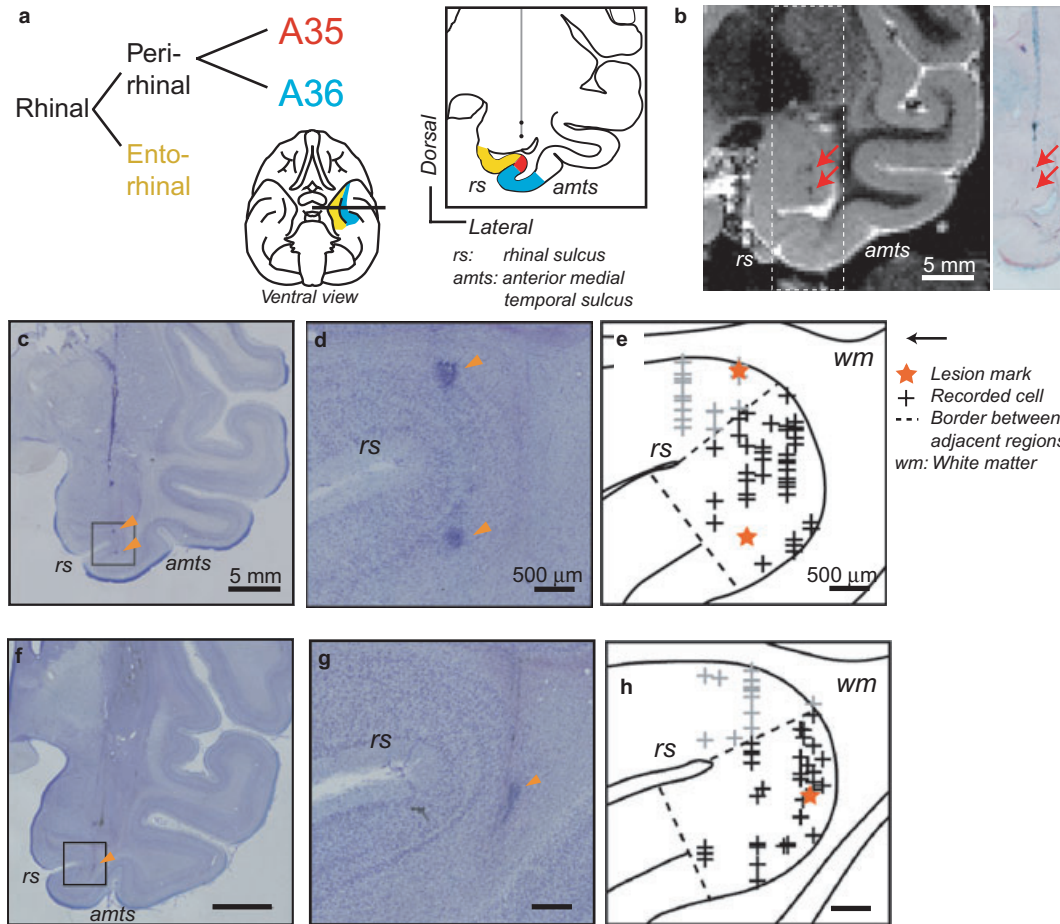
FIG. 1. Targeting A35 in a narrow strip of the fundus of the rhinal sulcus. (a) Left: anatomical subdivision of the rhinal cortex. Middle: ventral view of a monkey brain. Right: coronal plane indicated by the thick horizontal line on the ventral view. The vertical line indicates the track of an elgiloy microelectrode used to make reference metal deposits (dots) just above A35 (shown in red). (b) Left: detected metal deposits in an MR image (arrows). Right: metal deposits stained by Prussian-blue reaction in a corresponding histological section. (c) Nissl-stained section containing electrolytic lesions (arrowheads). (d) Magnified view of the area within the rectangle in (c). (e) Locations of recorded A35 neurons in the corresponding coronal plane (d). Star, lesion mark; crosses, recorded neurons; dashed lines, borders between adjacent regions. Note that the black cross indicates that the neuron was recorded from A35. (f–h) Reconstructed recording sites in another monkey. (f) Nissl-stained section with a lesion mark (arrowhead). (g) Magnified view of the area within the rectangle in (f). (h) Reconstructed recording sites in the corresponding coronal plane (f). Scale bars: 5 mm in (b, c and f); 500 μm in (d, e, g and h).
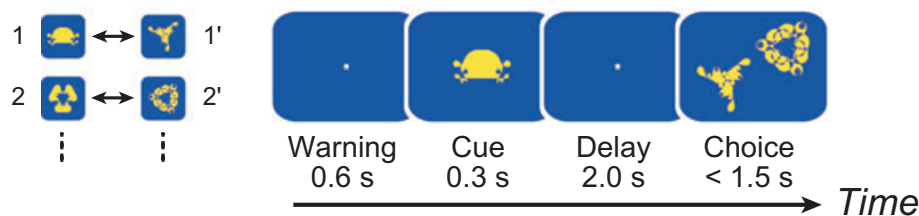

FIG. 2. PA task. In each trial a cue stimulus was presented, after which two choice stimuli, i.e. the paired associate of the cue stimulus (target) and a stimulus from a different pair (distractor), were sequentially presented with a delay of 2 s. The monkey obtained fruit juice as a reward for correctly touching the target within 1.5 s.

microlesions were made within A35 (Fig. 3, filled star and open star in the lower row). These microlesions near or within A35 enhanced the precision of the structural reconstruction, particularly accuracy in the depth dimension, and there was little distortion of the rhinal sulcus during the recording experiments. On the construction of the maps in Figs 1e and h, and 3, the position of recorded neurons was also confirmed by additional information from anatomical geometry (shape of sulci and thickness of gray matter). When estimating the position of a recorded neuron using Approach 2, a potential source of error arose

from the measurement of the microelectrode positions on the X-ray films (Yoshida et al., 2003). The error in the position on the maps was estimated to be similar to a SD of 0.18 mm (Yoshida et al., 2003). We therefore confirmed that none of the results in the present study changed when neurons situated within 0.18 mm of the borders between A35 and adjacent regions were excluded from the analysis. Coronal maps were made for each monkey; slice thicknesses were 1 mm, although some maps were merged across 2 mm for visualization purposes (Fig. 3).
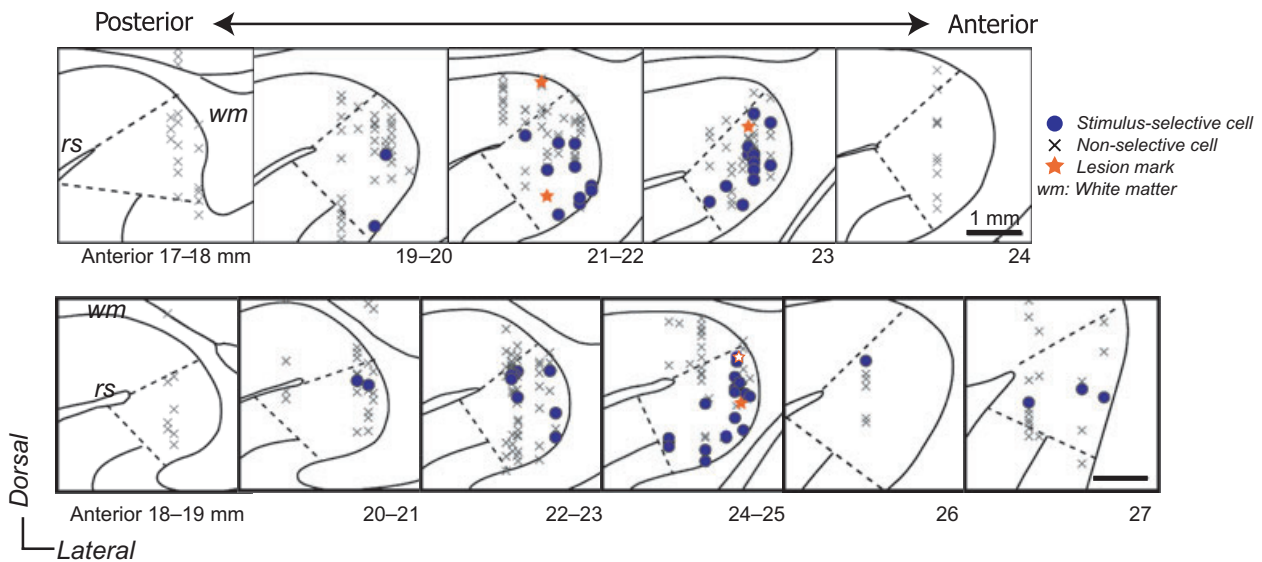
Posterior ←————————————————→ Anterior

FIG. 3. Spatial distribution of stimulus-selective cells in individual monkeys. Filled and open stars, lesion marks; crosses, non-selective cells; filled circles, stimulus-selective cells. In the lower row, the filled star corresponds to that in Fig. 1h and the open star indicates a lesion mark on another histological section. Scale bars: 1 mm.

Histology

After the placement of the last electrolytic lesion in each experiment, the monkeys were deeply anesthetized with sodium pentobarbital (60 mg/kg, i.v.) and then perfused intracardially with saline followed by 4% paraformaldehyde in 0.1 M phosphate buffer (pH 7.4). The brains were then removed, postfixed for 24 h in 4% paraformaldehyde at 4°C and cryoprotected in 30% sucrose in phosphate-buffered saline at 4°C until they sank. The brains were then cut into 40-μm cryostat sections in the coronal plane, so that the coronal sections corresponded to the coronal MR images acquired earlier. The sections were stained with cresyl violet (Nissl staining) or stained for iron using the Prussian blue reaction (Brown & Tasaki, 1961; Fung *et al.*, 1998) to visualize the metal deposits (Fig. 1b, right). Estimated shrinkage (5.0–9.0%) was corrected in each monkey, and histological sections were photographed using a BZ-9000 microscope and BZ-9000 software (Keyence, Tokyo, Japan). During their acquisition, the photomicrographic images were adjusted for brightness and contrast using the BZ-9000 software but were not otherwise altered.

The borders between A35 and adjacent regions were determined from the cytoarchitecture (Amaral *et al.*, 1987; Suzuki & Amaral, 2003a; Saleem *et al.*, 2007). A35 has a distinctive acellular band between layers III and V, whereas the lamina dissecans is not evident in the lateral entorhinal portion, the area medially adjacent to A35. The density of cells in layer VI is appreciably lower in A35 than in the lateral entorhinal portion, and layer VI shows no indication of lamination in A35, as it does in the lateral entorhinal portion. At the A35/A36 border, the lack of a granule cell layer in A35 distinguishes it from A36, which contains a sparse granule cell layer.

Data analysis

Stored data were analyzed off-line on a PC using MATLAB R14 (Mathworks) and SAS9.1 (SAS Institute Inc., NC, USA). The cue stimulus that elicited the strongest responses was referred to as the 'optimal stimulus' and the paired associate of the optimal stimulus was referred to as the 'pair stimulus'. The optimal and pair stimuli were referred to as the 'primary pair'. The trial in which the optimal stimulus was presented as a cue stimulus was referred to as the 'optimal trial'. The trial in which the pair stimulus was presented as a cue stimulus was referred to as the 'pair trial'. The trial in which each of the primary pair was presented as a cue stimulus was referred to as the 'primary trial'. The other 14 stimuli were referred to as the 'other stimuli'. The trials in which the other stimuli were presented as cue stimuli were referred to as 'other trials'. Pairs other than the primary pair were referred to as 'other pairs'.

Spike trains were smoothed by convolution with a Gaussian kernel (sigma = 30 ms) to obtain spike density functions. For each neuron, the neuronal response onset was determined as the time-point at which the spike density function in the optimal trials first exceeded 2 SD above the baseline activity, which was defined as the mean discharge rate for the 300-ms period immediately preceding the stimulus onset (Naya *et al.*, 2001). We defined the cue response as the firing rate during the period extending from 70 to 370 ms after cue onset; the first 70 ms was excluded to compensate for the minimum latency of visual responses in the temporal cortex (Xiang & Brown, 1998; Liu & Richmond, 2000). The firing rate during the last 1 s of the delay interval (1–2 s after cue offset) was measured as the delay activity.
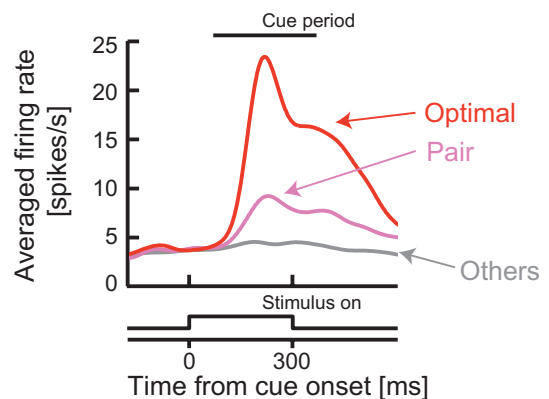

FIG. 4. Population-averaged responses for all cue-selective neurons in A35 ($n = 64$). Red, responses in the optimal trials; pink, responses in the pair trials; gray, responses in the other trials.

This time window was selected to exclude visual off responses and examine activity that had reached a stationary state. In addition to the cue response, we defined the 'initial response' as the averaged firing rate during the 300-ms period immediately after the response onset ('initial period'). For individual analyses in each neuron, the stimulus selectivity of responses during the cue, initial and delay periods for all of the stimuli was evaluated by one-way ANOVA ($P < 0.01$). In population analyses, the significance level was set at 5% unless otherwise stated.

The pair-coding index (PCI) was defined using a correlation coefficient as in Naya *et al.* (2003a): $\text{PCI} = \sum[(\chi_i - \mu)(\chi_i' - \mu')]/$ $[\sum(\chi_i - \mu)^2][\sum(\chi_i' - \mu')^2]^{1/2}$ ($i = 1$–8), where χ_i is the mean cue response for the i-th stimulus (the i-th and i'-th pictures belong to a pair) and μ and μ' are the averages of χ_i and χ_i'. If a single neuron in a population showed a pattern of stimulus selectivity that was independent of the stimulus pairs, the mean value of the PCI for the neuronal population would be expected to approach zero.

Receiver operating characteristic (ROC) analysis (Green & Swets, 1966; Yanike *et al.*, 2009) was conducted for stimulus-selective neurons to estimate their ability to discriminate within the primary pair comprised of the optimal stimulus and the pair stimulus. An ROC curve was constructed for each neuron by plotting the probability of correctly detecting one particular stimulus (probability of 'hits') as a function of the probability of misclassifying the other stimuli (probability of 'false alarms') across all decision thresholds. Thereafter, the area under the ROC curve (AUC) was computed, which gives a non-parametric measure of the separation of the responses to the two stimuli (Hanley & McNeil, 1982). The AUC value ranges between 0.5 and 1, with 1 equal to complete separation and values nearer 0.5 indicating responses that could not discriminate between the optimal stimulus and the pair stimulus. As a control, ROC analyses were also conducted for stimulus-selective neurons to estimate their ability to discriminate between the primary pair and the other pairs. The neuronal responses to the optimal stimulus and the pair stimulus were also compared for each stimulus-selective neuron using two-tailed *t*-tests ($P < 0.01$) to evaluate the difference between the two stimuli. The neuronal responses to the primary pair and the other pairs were similarly compared using two-tailed *t*-tests ($P < 0.01$).

In the present study, we analyzed A36 neurons in addition to A35 neurons. We used the A36 database in Naya *et al.* (2003a), which derived from three other monkeys performing a PA task. All A36 data were newly analyzed in the present study.

Results

Data set

We recorded from a total of 181 neurons in A35 of two monkeys performing a PA task (Fig. 2). Of these, 70 neurons showed response changes that exceeded 2 SD above the baseline activity for at least one stimulus among the 16 stimuli during either the cue presentation or the delay interval. Of them, 67 neurons showed significant ($P < 0.01$; one-way ANOVA) stimulus selectivity during the cue period (70–370 ms from cue onset) ($n = 64$) or delay period (the latter half of the delay interval) ($n = 18$). Collectively, these neurons will be referred to as being stimulus-selective. Among the 67 stimulus-selective neurons, 15 showed stimulus selectivity in both the cue and delay periods. The spatial distributions of stimulus-selective neurons in the coronal planes of each animal are illustrated in Fig. 3 (upper and lower rows, respectively). In both animals, most of the stimulus-selective neurons tended to cluster along the anteroposterior axis, extending from 21 to 23 mm or from 22 to 25 mm, respectively.

Pair-coding response

We found that the responses of cue-selective neurons in A35 to the paired associates were correlated in the PA task ('pair-coding response'), as previously seen with neurons in A36 (Naya *et al.*, 2003a). Figure 4 shows the population-averaged spike density functions of the A35 cue-selective neurons ($n = 64$) in the optimal trials (red line, mean ± SEM = 15.17 ± 0.85 Hz during the cue period), pair trials (pink line, 7.07 ± 0.89 Hz) and other trials (gray line, 4.31 ± 0.48 Hz) (for the definition of the optimal and pair trials, see Materials and methods). In this population, the paired associate of the optimal stimulus elicited a significantly stronger response than other stimuli (pair vs. other trials, $P = 0.0067$, paired-*t*-test).

The pair-coding response was also confirmed by using correlation between the responses to the paired associates. For each neuron, a correlation coefficient (PCI) was calculated between the mean firing rate during the cue period to one stimulus and that to its paired associate. We found that the distribution of the PCIs was shifted to the positive values in cue-selective neurons (median = 0.39, $P < 0.001$, Wilcoxon's signed-rank test). The shift to the positive values of PCIs in A35 neurons did not significantly ($P = 0.13$, Kolmogorov-Smirnov test) differ from those of the A36 neurons (A36, $n = 73$, median = 0.54), suggesting that, like A36 cue-selective neurons, A35 cue-selective neurons encode PA memory.

We also found that the pair-coding response was more prominent for the cue-selective neurons with stimulus-selective delay activity ($n = 15$, median PCI = 0.90) than for those without stimulus-selective delay activity ($n = 49$, median PCI = 0.17; Kolmogorov-Smirnov test, $P = 0.0021$) (Fig. 5, left). This tendency was also detected in A36 ($P = 0.0011$, Fig. 5, right), and the PCIs for the cue-selective neurons with stimulus-selective delay activity in A35 were not significantly different from those in A36 (Kolmogorov-Smirnov test, $P = 0.37$). This suggests that the delay-selective neurons in the both areas are involved in representing PA memories more closely than the neurons that did not maintain their stimulus selectivity as delay activity. Hereafter, we analyzed the neuronal activity of the delay-selective neurons in detail.

Unitized response

Figure 6a shows an example of a delay-selective neuron in A35. This neuron showed strong responses during the cue period in both the optimal (red line, mean ± SEM = 23.3 ± 4.26 Hz) and pair (pink line, 23.03 ± 2.77 Hz) trials. Notably, the amplitudes of this neuron's responses in the pair trials were similar to those in the optimal trials ($P = 0.71$, *t*-test), and this tendency continued into the delay period ($P = 0.50$).

The responses of another representative delay-selective neuron in A35 are shown in Fig. 6b. This neuron began responding near the end of the cue presentation and exhibited strong responses during the delay period in both the optimal (red line, 6.14 ± 0.78 Hz) and pair (pink line, 5.92 ± 1.03 Hz) trials. The amplitudes of this neuron's delay responses in the pair trials were also similar to those in the optimal trials ($P = 0.96$, *t*-test). Because some neurons showed a late response onset like the neuron in Fig. 6b, hereafter we used the initial period for analysis instead of the cue period to examine whether the responses of the primary pair in delay-selective neurons were similar from the beginning of their responses. The neuron in Fig. 6b showed similar responses to the optimal and pair stimuli within the primary pair during the initial period (4.62 ± 1.74 Hz for the optimal trials and 4.52 ± 0.86 Hz for the pair trials, $P = 0.86$). Only a small proportion of delay-selective neurons significantly distinguish the optimal trials from the pair trials ($P < 0.01$, *t*-test) during the initial period (16.7%)
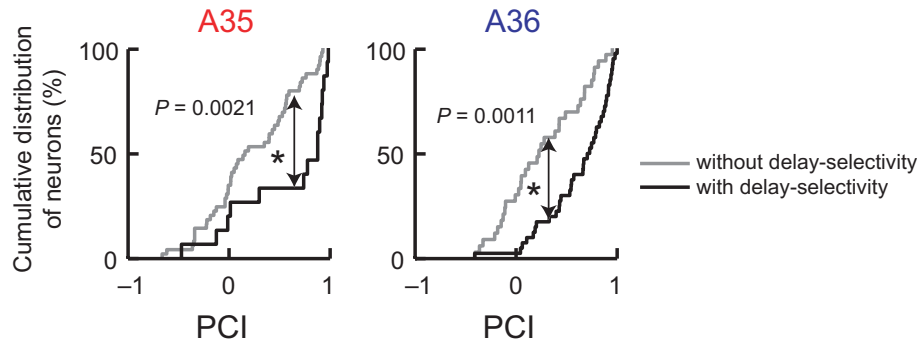
FIG. 5. Cumulative plot of PCI values in the cue-selective neurons showing delay selectivity and those without delay selectivity. The distributions of PCI values were significantly higher for cue-selective neurons with stimulus-selective delay activity (with delay selectivity, black line) than for those without stimulus-selective delay activity (without delay selectivity, gray line) in both A35 (left, Kolmogorov-Smirnov test, $P = 0.0021$) and A36 (right, $P = 0.0011$). The distributions of PCI values for cue-selective neurons with stimulus-selective delay activity did not significantly differ between A35 and A36 ($P = 0.21$).
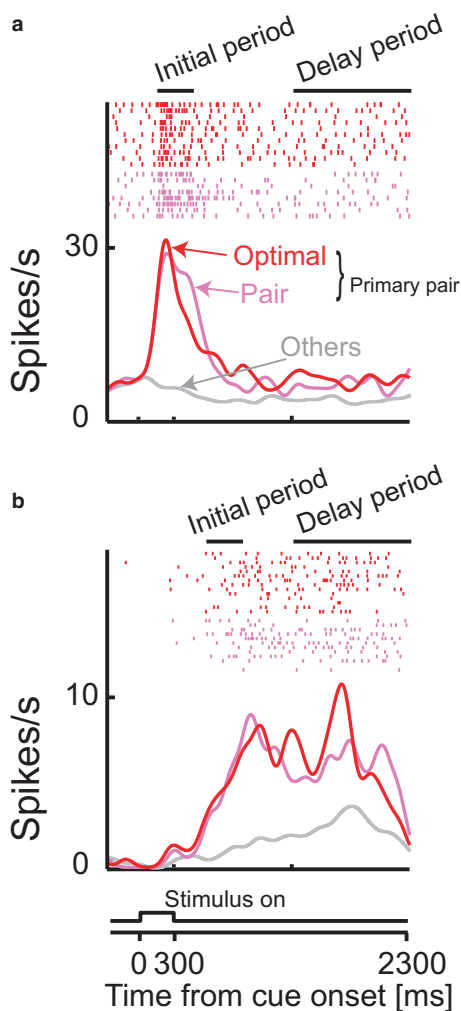

FIG. 6. Stimulus-selective responses elicited by paired associates in two representative A35 neurons. (a and b) Rastergrams and spike density functions for the optimal (red) and pair (pink) trials. The trials are aligned at the cue-stimulus onset. The gray line denotes the averaged responses in the other trials (others). A stimulus-selective response appeared during the cue-presentation period in (a), whereas the stimulus-selective response of the neuron in (b) had a later onset.

and the delay period (16.7%), indicating that the majority of delay-selective neurons showed similar responses in the primary pair. These similar responses seemed to be unique for delay-selective neurons in

A35 because, in A36, 72.5 and 42.5% of delay-selective neurons showed significantly different responses to the optimal and pair trials (during the initial and delay period, respectively), although their PCI values were as high as those of A35 (Fig. 5, right).

We next examined whether the neuronal activity could discriminate between the optimal and pair trials while retaining selective responses to the primary pair. This pattern of neuronal activity was referred to here as the 'unitized response'.

We confirmed these tendencies by performing an ROC analysis, through which we estimated each neuron's ability to discriminate optimal trials from pair trials. In A35, the median values of the AUC for discrimination within the primary pair were 0.76 and 0.65 during the initial and delay periods, respectively, whereas the median values of AUCs in A36 were 0.96 and 0.79, respectively. Thus, AUCs were significantly smaller in A35 than A36 during both the initial and delay periods (Fig. 7a, Kolmogorov-Smirnov test, $P = 0.0042$ and 0.02, respectively). This means that the responses in the optimal and pair trials were less distinguishable in A35 than in A36.

We next estimated each neuron's ability to discriminate the primary pair from the other pairs. We found that AUCs for the discrimination between the primary pair and other pairs did not significantly differ between A35 (median = 0.91 and 0.72 during the initial and delay periods, respectively) and A36 (median = 0.94 and 0.72) during either the initial or delay period (Fig. 7b, Kolmogorov-Smirnov test, $P = 0.40$ and 0.92, respectively). This means that neurons in both A35 and A36 retained selective responses to the primary pair.

In summary, these results indicate that delay-selective neurons in A35 exhibited more unitized responses than those in A36 and that these unitized responses were retained from the response onset to the end of the delay period.

Discussion

By combining MRI-guided *in-vivo* localization with postmortem histological localization of the recording sites, we were able to overcome the technical difficulty of targeting A35 neurons and systematically record from A35 in behaving monkeys. In A35 cue-selective neurons, we found that the responses to one stimulus strongly correlated with those to the paired associate, indicating that PA memory was represented in A35, as it was in A36. In both areas, these correlations were stronger in cue-selective neurons that also showed delay selectivity than in those without delay selectivity. The delay-selective neurons in A35 distinguish the primary pair from other pairs as well as those in A36 but the ability to discriminate

a
Optimal vs pair trials
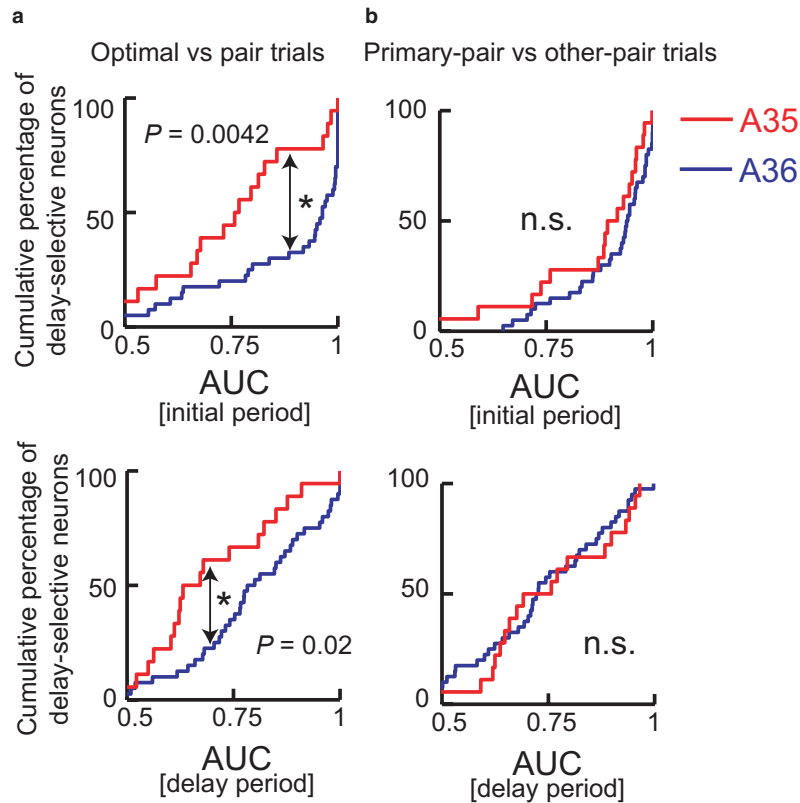
b
Primary-pair vs other-pair trials

FIG. 7. Comparison of AUCs between A35 and A36. (a) The AUCs for the optimal and pair stimuli were smaller for delay-selective neurons in A35 than A36 during both the initial (upper) and delay (lower) periods (Kolmogorov-Smirnov test, $P = 0.0042$ and $P = 0.02$, respectively). This means that responses to optimal and pair stimuli were more similar for delay-selective neurons in A35 than in A36. Red lines, A35; blue lines, A36. (b) The AUCs for the primary pair and other pairs during both periods did not differ between the two areas ($P = 0.40$, $P = 0.92$, respectively), indicating that selectivity among pairs did not differ in A35 and A36.
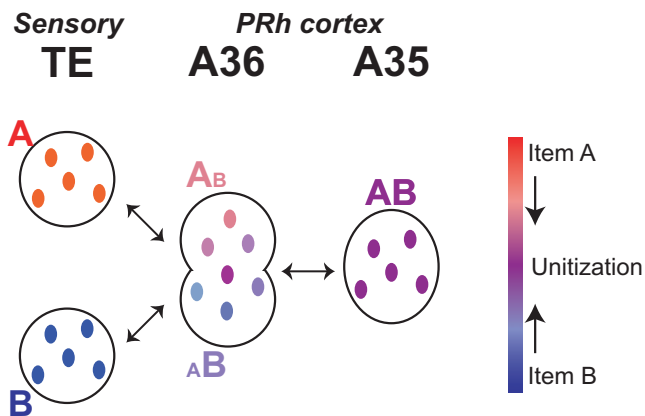

FIG. 8. Schematic drawing of the hierarchical processing for item unitization in the PRh cortex. An object A and its paired associate, an object B, are complex but geometrically-unrelated objects. In sensory areas on the ventral visual pathway (such as area TE), when these two objects are presented as a cue stimulus, a group of neurons (colored dots in red or blue) respond to either A or B. In A36, neurons respond to both items, although the response amplitude is biased to one or the other of the pair. Thus, these neurons represented PA memory as two associated stimuli. In A35, by contrast, neurons respond equally to both items. Thus, the pair is represented as a single unitized item (colored in purple), i.e. A35 represents PA memory at a more abstract level than A36 does.

within the primary pair (i.e. between the optimal and pair stimuli) significantly differed between the two areas; responses of delay-selective A35 neurons to the optimal and pair stimuli were similar, whereas responses of the delay-selective A36 neurons discriminated

between the optimal and pair stimuli. These results suggest that A35 delay-selective neurons treat the two stimuli as a single unitized item, and thus represent PA memory at a more abstract level than those in A36.

Strategy for targeting area 35

In the macaque inferior temporal cortex, using X-ray images of the electrodes (Higuchi & Miyashita, 1996; Messinger *et al.*, 2001; Naya *et al.*, 2003a) or structural MR images (Janssen *et al.*, 2001; Sheinberg & Logothetis, 2001) enabled us to localize the recording sites within target areas with the necessary accuracy. However, because A35 is a narrow strip on the fundus of the rhinal sulcus with no lining structure (e.g. dura mater or bone) and the boundary between layer VI in A35 and the subcortical white matter is diffuse in appearance (Suzuki & Amaral, 2003a), it is difficult to uniquely determine the microelectrode position with each physiological recording profile. Only one *in-vivo* study has been performed, recording spontaneous neuronal activity from the cat A35 by simultaneously implanted electrodes across the rhinal cortex (Pelletier *et al.*, 2004). Recently, several *in-vivo* methods have been proposed for improving the accuracy with which microelectrode position can be detected (Matsui *et al.*, 2007; Cox *et al.*, 2008). In the present study, we improved the accuracy by overlaying and aligning the recording profiles on high-resolution MR images using MR-detectable markers (Fung *et al.*, 1998; Koyano *et al.*, 2008).

By combining MRI-detectable markers and histological confirmation, we were able to accomplish A35 mapping and to functionally

distinguish A35 from adjacent areas. We found that stimulus-selective neurons tended to cluster together within A35. The majority were situated within 3–4 mm of each other along the anteroposterior axis but were not necessarily distributed near the border with A36 or the entorhinal cortex. Stimulus-selective neurons in A36 are also localized within a focal patch around the medial lip of the anterior middle temporal sulcus (Naya *et al.*, 2003a; Yoshida *et al.*, 2003). Because this focal patch in A36 is not located near the border between A35 and A36, we concluded that the clustering region that we observed in A35 was distinct from the focal patch in A36.

The application of the method described in the present study is not limited to recording from macaque A35. Indeed, we suggest that this two-track approach could be of benefit in other electrophysiological studies carried out *in vivo* or in awake monkeys, as it enables us to accomplish fine mapping that could distinguish target areas from adjacent areas and generally more accurate determination of where the recording sites are situated.

Functional similarities and difference between areas 35 and 36 during the pair-association task

Our earlier finding that the PCI values for neurons in A36 were significantly higher than for neurons in area TE (i.e. outside the PRh cortex) suggests that association between the representations of the paired associates proceeds forward from area TE to A36 (Naya *et al.*, 2003a). In the present study, we took one more step along a hierarchical pathway to examine the functional properties of A35, and found that representation of PA memory proceeds further within the PRh cortex from A36 to A35, whereas the pair-coding property itself was similar between A35 and A36.

Within A35, delay-selective neurons showed a pair-coding response throughout the trials (Fig. 6a and b) but the activity of these neurons during the delay period did not discriminate between the optimal and pair trials. By contrast, the activities of each delay-selective neuron in A36 clearly discriminated the optimal trials from the pair trials during the delay period, as previously reported by exhibiting two types of activity, a 'cue-holding response' (Fig. S1a) and a 'pair-recall response' (Fig. S1b) (Naya *et al.*, 2003b). In neurons showing the cue-holding response, the response amplitude in the optimal trials during the delay period was larger than that in the pair trials (Fig. S1a). However, in neurons showing the pair-recall response, the response amplitude in the pair trials during the delay period was larger than that in the optimal trials (Fig. S1b). Although individual A36 delay-selective neurons discriminated the optimal stimulus from its paired associate, at the population level of A36, the averaged delay activities in the optimal trials during the delay period did not significantly differ from those in the pair trials (Naya *et al.*, 2003b). In the present study, similar responses to the optimal stimulus and its paired associate were observed in A35 at the individual cell level.

Functional role of unitized response

Unitization is a condition in which two or more separate items or stimulus components are represented as a single unit (Graf & Schacter, 1989). A recent human imaging study showed that activation in the PRh cortex was increased when subjects encoded a pair of objects as a single item rather than two separate but associated items (Haskins *et al.*, 2008), which suggests that unitization relies on the PRh cortex. We found that delay-selective neurons in A35 showed similar responses to the optimal and pair stimuli, whereas these neurons retained selectivity between the pairs. We named this response pattern

a unitized response. Our findings provide direct evidence that unitization is represented at the individual cell level in A35. Moreover, the differential representations of pair-associative memory between A35 and A36 suggest that A35 represents PA memory at a more abstract level than A36, and that the two subdivisions of the PRh cortex (i.e. A35 and A36) establish a hierarchical organization for item unitization processing (Fig. 8).

In addition to a role of memory function, such as associative recognition via unitization of items, the previous studies also suggested that the PRh cortex maintains complex stimulus representations as part of the ventral visual stream hierarchy (Buckley & Gaffan, 1998; Murray *et al.*, 2007). It was theoretically predicted that the PRh cortex would functionally contribute to both the ventral visual stream and the medial temporal lobe memory system (Bunsey & Eichenbaum, 1993; Bussey & Saksida, 2007) on the basis of not only anatomical connectivity studies (Amaral *et al.*, 1987; Suzuki & Amaral, 2003b) but also behavioral and lesion studies (Buckley *et al.*, 2001; Bussey *et al.*, 2002; Barense *et al.*, 2005). For example, Bussey *et al.* (2002) showed that lesions of the macaque PRh cortex impair performance of a biconditional discrimination task that requires an association between complex component stimuli. The result suggests that, to solve this task, the PRh cortex supports the conjunctive representations as a specific combination of the complex components via associative memory. Buckley *et al.* (2001) demonstrated that bilateral PRh cortex lesions in macaques impaired perceptual discrimination between stimuli (such as degraded objects or scenes containing objects) when the discrimination requires processing of stimuli with multiple features at an 'object' level. Our present results suggest that these conjunctive representations/ object representations could be implemented by the network of A35 neurons that acquire abstract information about associative relationships among multiple objects or multiple features in a complex scene. It is tempting to see whether future advancements in lesion studies can reveal functional differentiation between A35 and A36, as suggested by our present neurophysiological study.

Supporting Information

Additional supporting information may be found in the online version of this article:

Fig. S1. Stimulus-selective responses to both paired associates of representative A36 neurons.

Please note: As a service to our authors and readers, this journal provides supporting information supplied by the authors. Such materials are peer-reviewed and may be re-organized for online delivery, but are not copy-edited or typeset by Wiley-Blackwell. Technical support issues arising from supporting information (other than missing files) should be addressed to the authors.

Acknowledgements

Abbreviations

A35, area 35; A36, area 36; AUC, area under the receiver operating characteristic curve; MR, magnetic resonance; MRI, magnetic resonance imaging; PA, pair-association; PCI, pair-coding index; PRh, perirhinal; ROC, receiver operating characteristic.

References

Amaral, D.G., Insausti, R. & Cowan, W.M. (1987) The entorhinal cortex of the monkey: I. Cytoarchitectonic organization. *J. Comp. Neurol.*, **264**, 326–355.

Barense, M.D., Bussey, T.J., Lee, A.C.H., Rogers, T.T., Davies, R.R., Saksida, L.M., Murray, E.A. & Graham, K.S. (2005) Functional specialization in the human medial temporal lobe. *J. Neurosci.*, **25**, 10239–10246.

Brown, K.T. & Tasaki, K. (1961) Localization of electrical activity in the cat retina by an electrode marking method. *J. Physiol.*, **158**, 281–295.

Buckley, M.J. & Gaffan, D. (1998) Perirhinal cortex ablation impairs visual object identification. *J. Neurosci.*, **18**, 2268–2275.

Buckley, M.J., Booth, M.C., Rolls, E.T. & Gaffan, D. (2001) Selective perceptual impairments after perirhinal cortex ablation. *J. Neurosci.*, **21**, 9824–9836.

Buffalo, E.A., Ramus, S.J., Clark, R.E., Teng, E., Squire, L.R. & Zola, S.M. (1999) Dissociation between the effects of damage to perirhinal cortex and area TE. *Learn. Mem.*, **6**, 572–599.

Bunsey, M. & Eichenbaum, H. (1993) Critical role of the parahippocampal region for paired-associate learning in rats. *Behav. Neurosci.*, **107**, 740–747.

Bussey, T.J. & Saksida, L.M. (2005) Object memory and perception in the medial temporal lobe: an alternative approach. *Curr. Opin. Neurobiol.*, **15**, 730–737.

Bussey, T.J. & Saksida, L.M. (2007) Memory, perception, and the ventral visual-perirhinal-hippocampal stream: thinking outside of the boxes. *Hippocampus*, **17**, 898–908.

Bussey, T.J., Saksida, L.M. & Murray, E.A. (2002) Perirhinal cortex resolves feature ambiguity in complex visual discriminations. *Eur. J. Neurosci.*, **15**, 365–374.

Cho, K., Kemp, N., Noel, J., Aggleton, J.P., Brown, M.W. & Bashir, Z.I. (2000) A new form of long-term depression in the perirhinal cortex. *Nat. Neurosci.*, **3**, 150–156.

Cox, D.D., Papanastassiou, A.M., Oreper, D., Andken, B. & DiCarlo, J.J. (2008) High-resolution three-dimensional microelectrode brain mapping using stereo microfocal x-ray imaging. *J. Neurophysiol.*, **100**, 2966–2976.

de Curtis, M. & Paré, D. (2004) The rhinal cortices: a wall of inhibition between the neocortex and the hippocampus. *Prog. Neurobiol.*, **74**, 101–110.

Fung, S.H., Burstein, D. & Born, R.T. (1998) *In vivo* microelectrode track reconstruction using magnetic resonance imaging. *J. Neurosci. Methods*, **80**, 215–224.

Graf, P. & Schacter, D.L. (1989) Unitization and grouping mediate dissociations in memory for new associations. *J. Exp. Psychol. Learn. Mem. Cogn.*, **15**, 930–940.

Green, D.M. & Swets, J.A. (1966) *Signal Detection Theory and Psychophysics*. Wiley and Sons, New York.

Hanley, J.A. & McNeil, B.J. (1982) The meaning and use of the area under a receiver operating characteristic (ROC) curve. *Radiology*, **143**, 29–36.

Haskins, A.L., Yonelinas, A.P., Quamme, J.R. & Ranganath, C. (2008) Perirhinal cortex supports encoding and familiarity-based recognition of novel associations. *Neuron*, **59**, 554–560.

Higuchi, S. & Miyashita, Y. (1996) Formation of mnemonic neuronal responses to visual paired associates in inferotemporal cortex is impaired by perirhinal and entorhinal lesions. *Proc. Natl Acad. Sci. USA*, **93**, 739–743.

Janssen, P., Vogels, R., Liu, Y. & Orban, G.A. (2001) Macaque inferior temporal neurons are selective for three-dimensional boundaries and surfaces. *J. Neurosci.*, **21**, 9419–9429.

Koyama, M., Hasegawa, I., Osada, T., Adachi, Y., Nakahara, K. & Miyashita, Y. (2004) Functional magnetic resonance imaging of macaque monkeys performing visually guided saccade tasks: comparison of cortical eye fields with humans. *Neuron*, **41**, 795–807.

Koyano, K.W., Machino, A., Fujimichi, R., Takeda, M., Ohashi, Y., Matsui, T. & Miyashita, Y. (2008) Electrolysis of an elgiloy electrode can create MRI-visible metal deposit marks at recording sites. The 38th Annual Meeting of Society for Neuroscience, On-line abstract # 885.2.

Liu, Z. & Richmond, B.J. (2000) Response differences in monkey TE and perirhinal cortex: stimulus association related to reward schedules. *J. Neurophysiol.*, **83**, 1677–1692.

Matsui, T., Koyano, K.W., Koyama, M., Nakahara, K., Takeda, M., Ohashi, Y., Naya, Y. & Miyashita, Y. (2007) MRI-based localization of electrophysiological recording sites within the cerebral cortex at single-voxel accuracy. *Nat. Methods*, **4**, 161–168.

Messinger, A., Squire, L.R., Zola, S.M. & Albright, T.D. (2001) Neuronal representations of stimulus associations develop in the temporal lobe during learning. *Proc. Natl Acad. Sci. USA*, **98**, 12239–12244.

Miyashita, Y. (1988) Neuronal correlate of visual associative long-term memory in the primate temporal cortex. *Nature*, **335**, 817–820.

Miyashita, Y. (1993) Inferior temporal cortex: where visual perception meets memory. *Annu. Rev. Neurosci.*, **16**, 245–263.

Miyashita, Y. (2004) Cognitive memory: cellular and network machineries and their top-down control. *Science*, **306**, 435–440.

Murray, E.A., Gaffan, D. & Mishkin, M. (1993) Neural substrates of visual stimulus-stimulus association in rhesus monkeys. *J. Neurosci.*, **13**, 4549–4561.

Murray, E.A., Bussey, T.J. & Saksida, L.M. (2007) Visual perception and memory: a new view of medial temporal lobe function in primates and rodents. *Annu. Rev. Neurosci.*, **30**, 99–122.

Naya, Y., Yoshida, M. & Miyashita, Y. (2001) Backward spreading of memory-retrieval signal in the primate temporal cortex. *Science*, **291**, 661–664.

Naya, Y., Yoshida, M. & Miyashita, Y. (2003a) Forward processing of long-term associative memory in monkey inferotemporal cortex. *J. Neurosci.*, **23**, 2861–2871.

Naya, Y., Yoshida, M., Takeda, M., Fujimichi, R. & Miyashita, Y. (2003b) Delay-period activities in two subdivisions of monkey inferotemporal cortex during pair association memory task. *Eur. J. Neurosci.*, **18**, 2915–2918.

Pelletier, J.G., Apergis, J. & Pare, D. (2004) Low-probability transmission of neocortical and entorhinal impulses through the perirhinal cortex. *J. Neurophysiol.*, **91**, 2079–2089.

Sakai, K. & Miyashita, Y. (1991) Neural organization for the long-term memory of paired associates. *Nature*, **354**, 152–155.

Saleem, K.S., Price, J.L. & Hashikawa, T. (2007) Cytoarchitectonic and chemoarchitectonic subdivisions of the perirhinal and parahippocampal cortices in macaque monkeys. *J. Comp. Neurol.*, **500**, 973–1006.

Sheinberg, D.L. & Logothetis, N.K. (2001) Noticing familiar objects in real world scenes: the role of temporal cortical neurons in natural vision. *J. Neurosci.*, **21**, 1340–1350.

Suzuki, W.A. & Amaral, D.G. (2003a) Perirhinal and parahippocampal cortices of the macaque monkey: cytoarchitectonic and chemoarchitectonic organization. *J. Comp. Neurol.*, **463**, 67–91.

Suzuki, W.A. & Amaral, D.G. (2003b) Where are the perirhinal and parahippocampal cortices? A historical overview of the nomenclature and boundaries applied to the primate medial temporal lobe. *Neuroscience*, **120**, 893–906.

Xiang, J.Z. & Brown, M.W. (1998) Differential neuronal encoding of novelty, familiarity and recency in regions of the anterior temporal lobe. *Neuropharmacology*, **37**, 657–676.

Yanike, M., Wirth, S., Smith, A.C., Brown, E.N. & Suzuki, W.A. (2009) Comparison of associative learning-related signals in the macaque perirhinal cortex and hippocampus. *Cereb. Cortex*, **19**, 1064–1078.

Yoshida, M., Naya, Y. & Miyashita, Y. (2003) Anatomical organization of forward fiber projections from area TE to perirhinal neurons representing visual long-term memory in monkeys. *Proc. Natl Acad. Sci. USA*, **100**, 4257–4262.